Maximum Likelihood Estimators for Three-Dimensional Rigid Body Localization in Internet of Things Environments

LINGYU AI[1], CHANGQIANG JING[2], YEHCHENG CHEN[3], SHENGLAN WU[1], AND TAO ZHANG[1], (Member, IEEE)
[1]IoT Engineering Research Center of the Ministry of Education, Jiangnan University, Wuxi 214122, China
[2]Department of Informatics, Linyi University, Linyi 276000, China
[3]Department of Computer Science, University of California at Davis, Davis, CA 95616, USA

Corresponding author: Changqiang Jing (jingchangqiang@lyu.edu.cn)

ABSTRACT Different from the conventional point source localization, rigid body localization (RBL) not only aims to estimate the position of the target but also to acquire the attitude information, which is also essential information in many Internet of Things (IoT) applications, such as the virtual reality systems, smart parking systems. This paper develops three maximum likelihood estimators (MLEs) for the RBL purpose in 3 dimensional space via a single base station. The MLEs are designed for the RBL framework, which adopts the direction of arrival (DoA) of the signal from a small scale wireless sensor network (SSWSN) mounted on the surface of the rigid target as measurement and can be realized by a single base station. The three MLEs respectively exploit the SSWSN topology information, the DoA measurement information only, as well as the equality constraint of the rotation matrix and the DoA measurement information. In addition, we implement the modified Guass-newton algorithm for the MLEs of the rotation matrix and the translation vector. Simulations show that the proposed MLE fusing the equality constraint of the rotation matrix and the DoA measurement information most approaches the Cramer-Rao Lower Bound and also outperforms the other two MLEs in terms of convergence success rate and the computational cost.

INDEX TERMS Internet of Things (IoT), maximum likelihood estimator, rigid body localization, direction of arrival, convergence success rate.

I. INTRODUCTION

A target with a rigid body refers to an object that remains the same topological structure in motion or under force. It can be extended to many types of Internet of Things (IoT) objects, such as spacecraft, helmets used in Virtual Reality (VR) or intelligent robots, etc. The rigid body localization (RBL) including the rigid body positioning and orientation estimation scheme, are uesd to estimate central coordinate and the rotation Euler angles (pitch, yaw, roll) of a rigid body to a reference state [1]–[4].

High-precision position and posture information of the rigid body play an important role as basis in aerospace, military, intelligent industrial systems and other IoT applications [5]–[7]. In VR applications, the VR system provide

The associate editor coordinating the review of this manuscript and approving it for publication was Mu-Yen Chen.

corresponding virtual pictures according to the accurate position and posture of the user's head [8]–[9]. In the indoor precise navigation system [10], the position and orientation of vehicles are the fundamental information for the intelligent parking system. The precious posture and relative position information of a spacecraft is needed for the space docking mechanism. In one word, the RBL scheme has an extensive application in the future.

As the mainstream position and orientation estimation technology of large-scale rigid body, the Global Navigation Satellite System (GNSS) can compute the absolute position of the rigid body according to the distance intersection of pseudo-range observation. Meanwhile, the orientation information can be determined by using the baseline vector's orientation in space of carrier phase measurements [11], [12]. However, the integer ambiguity resolution involved in satellite carrier phase affects the stability of this scheme.

Besides, the effectiveness of satellite positioning cannot be guaranteed in indoor, underwater, tunnel, mine, and other non-line of sight environments. What's more, complex satellite receiving antenna system also leads to high implementation costs for this solution.

The position and orientation estimation scheme using visual image processing is another popular solution of passive tracking system [13]–[16]. In this scheme, the absolute position and orientation information can be obtained by singular value decomposition [14], orthogonal decomposition [15], unit quaternion algorithms based on 3 dimensional (3-D) coordinate of feature points observed by single or multiple theodolites. However, the positioning accuracy of this scheme excessively depends on low error coordinate observation value of feature points. The technical characteristics of visual image processing also lead to poor robustness of light conditions and high computational cost, limiting engineering application.

In common IoT environments, the positioning and orientation estimation scheme of a rigid body based on small-scale wireless sensor network (SSWSN) has the advantages of low implementation cost, strong adaptability to indoor-outdoor environments and light conditions [17]–[21]. The implementation of an estimation scheme based on small-scale WSN can be concluded as follows: First, the wireless sensing node is attached to the surface of the rigid body forming a small-scale sensing network with known topology size. Secondly, the physical observation of each wireless node in the network will be obtained at the base station. Meanwhile, the scheme will establish a mathematic model based on the prior knowledge of the topology of the wireless nodes. Finally, the three-dimensional coordinates and orientation information of the rigid body are obtained through optimization algorithms. Currently, the research approaches of positioning and orientation estimation scheme based on the wireless sensor network mainly focuses on range-based observation, including a time difference of arrival (TDoA) and time of arrival (ToA). The scheme employs distance between each node-pairs of SSWSN and range-based observation captured by the base stations to form the mathematic model. While the relative position of each wireless node in the topology network is already known. The absolute position of each node can be estimated in two steps, First, by the affine transform, the schemes obtain the multiplication of relative position coordinate and the unknown special orthogonal group. Second, the scheme adds the unknown translation vector relative to the origin of the inertial reference point and multiplication relatived to the origin of the inertial reference base together. Finally, the scheme will establish an attitude and position estimation model by matching ToA observations from all nodes to each base station with estimated translation vectors. However, how to optimize this model is a much more challenging problem because of the constraint that the three-dimensional special orthogonal group containing pose information satisfy the unit orthogonal condition of the unitary matrix [23]–[26]. Plenty of optimization algorithms

can be adopted for the optimization problem [27]–[32], such as particle swarm optimization (PSO) algorithm, maximum likelihood estimation (MLE) algorithm, as well as the Semidefinite Relaxation Method, etc. However, to ensure the accuracy of the system, a range-based wireless sensor network positioning scheme requires 4-5 base stations, which increases the implementation cost of the system. The practicability of the ToA-based positioning and attitude estimation scheme is not well because of the strict clock synchronization problem between the base station and sensor node. While, direction of arrival (DoA) Observations based on positioning and attitude estimation scheme can completely avoid the clock synchronization problem, improving the feasibility of the system [33]. Besides this, the two-dimensional DoA information obtained at the base station has a higher dimension than ToA information, which makes it possible to locate orientation with a single base station.

The DoA-based RBL model using a single base station has important practical significance in many military areas. For example, the Airborne Warning and Control System (AWACS) equipped with phased array radar usually plays the role of commander of other combat aircraft in air combat under electronic interference circumstances. While single AWACS combat system effectively reduce combat costs and system complexity. The steering vector is captured by Antenna Array when the signal is injected on a phased array radar. After that, the location information of the signal source will be obtained by the DoA estimation algorithm. Among all kinds of DoA estimation methods, the multiple signal classification algorithm based on feature decomposition has obvious accuracy advantage and has been a mature technology currently [34], [35]. The authors of [21] first proposed a DoA based RBL scheme. They divided the RBL work into two steps: using the PSO algorithm to locate the SSWSN nodes and getting the rotation matrix (attitude) and the translation vector (position) through the singular value decomposition (SVD) algorithm. However, the PSO algorithm is not so efficient in terms of optimization success rate and computational cost. Reference [22] used the semidefinite relaxation method (SR) for DoA based RBL work, however an additional refinement is required using the maximum likelihood estimation algorithm, and this solution only is proved to be efficient under low measurement condition.

Based on the background above, in this paper, we make the following contributions:

1. We propose three maximum likelihood estimates for DoA based RBL work: the first one adopts the topology information matching to form a topology maximum likelihood estimate; the second adopts the DoA measurement matching to form an observation maximum likelihood estimate; and the third fuses the DoA measurement and the constraint of the rotation matrix to form a combined maximum likelihood estimate.

2. We modified the Guassian-Newdon algorithm for the three MLEs. All three maximum likelihood estimates are optimized by the modified Gaussian-Newton
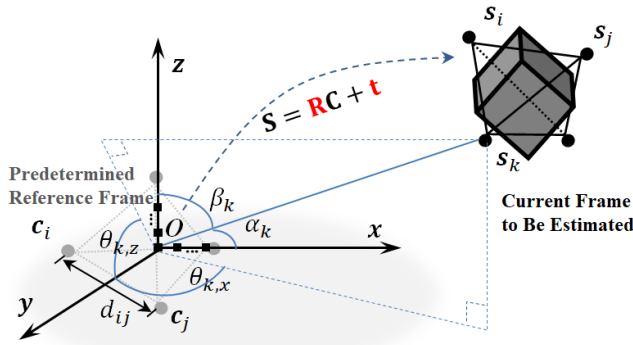
FIGURE 1. The current state of the rigid target is assumed to be rotated and moved from the Reference frame.

algorithm with an additional convergence quality check to avoid the local optimization convergence.

The following of the paper is organized as follows: Section II describes of the DoA-based Rigid body Location Framework, in which the conditions and the parameters for three maximum likelihood estimates are mentioned. In Section III, the maximum likelihood estimators for DoA-based RBL framework are discussed in detail, according to the conditions' distribution characteristics. The modified Gaussian-Newton algorithm for the MLEs is presented while providing the necessary information for optimization implementation in Section IV. Performance evaluation is conducted in Section V, in which the three MLE are compared in terms of optimization success rate and convergence success, meanwhile the estimation accuracy of proposed methods is evaluated comparing with the constraint Cramer-Rao bound (CCRB). Finally, the conclusion and future work are given in Section VI.

II. DoA-BASED RIGID BODY LOCATION FRAMEWORK

This section introduce the RBL framework based on the DoA measurement, with only one single BS. To determine the state (including the position and the attitude) of the rigid body in 3-D space, K wireless nodes, forming a small scale wireless sensor network, are mounted on its surface as feature points. The topology information of the SSWSN is exactly known in advance and remains unchanged while moving and in the rotation.

Without loss of generality, the single base station is set as the origin O. The single base station will receive the signal from each node in the SSWSN and then measure the signal arriving direction. For DoA measuring, the BS is equipped with a 2 dimensional (2-D) antenna array to measure DoA information with two dimensional including azimuth angle and the elevation angle; as shown in Figure 1, we assume that the 2-D antenna array is distributed uniformly along x-axis and z-axis, respectively. The size effect of the antenna array can be ignored although we enlarge the antenna array in the figure for clearer illustration, and the incoming signals are paralleled.

The state of the rigid target to be estimated is represented by the current state of the SSWSN, which is termed the

current frame. To describe the state of the current frame of the SSWSN, we are to predefine a reference frame. The current frame is obtained from the reference frame by undergoing rotation and a translation, which is mathematically expressed as

$$\mathbf{S} = \mathbf{RC} + \mathbf{t} \otimes 1^{1 \times K}. \tag{1}$$

where $\mathbf{C} = [\mathbf{c}_1, \ldots, \mathbf{c}_K] \in \mathbb{R}^{3 \times K}$ and $\mathbf{S} = [\mathbf{s}_1, \ldots, \mathbf{s}_K] \in \mathbb{R}^{3 \times K}$ represent the reference frame and the current frame respectively. In $\mathbf{C}$ and $\mathbf{S}$, the kth node's 3-D coordinate position is $\mathbf{c}_k = [c_{x,k}, c_{y,k}, c_{z,k}]^T$ and $\mathbf{s}_k = [s_{x,k}, s_{y,k}, s_{z,k}]^T$, respectively. In (1), $\mathbf{t} = [x, y, z]^T$ is the unknown translation vector and $\mathbf{R}$ is the unknown rotation matrix and orthogonal matrix belonging to a 3-D special orthogonal matrix

$$SO(3) = \{\mathbf{R} \in \mathbb{R}^{3 \times 3} : \mathbf{RR}^T = \mathbf{R}^T \mathbf{R} = I_3, \det(R) = 1\}. \tag{2}$$

For the generalized RBL problem, the task is to find the rotation matrix $\mathbf{R}$ and the translation vector $\mathbf{t}$. However, estimating $\mathbf{R}$ and $\mathbf{t}$ is a challenging problem because of the constraint (2).

The topology information is prior knowledge that can be used for estimating $\mathbf{R}$ and $\mathbf{t}$. Since the topology information remains unchanged, if we can describe the topology information using the Euclidean distances of the node pairs

$$\mathbf{d} = [d_{1,2}, \ldots, d_{i,j}, \ldots, d_{K-1,K}]^T, \quad i, j = 1, \ldots, K, i > j, \tag{3}$$

where $d_{i,j} = \|\mathbf{c}_i - \mathbf{c}_j\| = \|\mathbf{s}_i - \mathbf{s}_j\|$ is the Euclidean distance between the ith and jth node. $\mathbf{d}$ is an $\frac{K(K-1)}{2} \times 1$ vector when a full connected scenario is considered.

The other condition is the measured DoAs. The angles between the arrival signal of k-th node in the current frame $\mathbf{s}_k$ and the x- and z-axes, α_k and β_k, can be measured. For facilitation, we convert α_k and β_k into the projected azimuth angle $\theta_{k,x}$ and the projected pitch angle $\theta_{k,z}$ that

$$\begin{cases} \theta_{k,x} = \arctan \sqrt{\dfrac{\tan^2 \beta_k + 1}{\tan^2 \alpha_k \tan^2 \beta_k - 1}} \\ \theta_{k,z} = \arctan \sqrt{\dfrac{\tan^2 \alpha_k + 1}{\tan^2 \alpha_k \tan^2 \beta_k - 1}}. \end{cases} \tag{4}$$

We define the collection of $\theta_{k,x}$ and $\theta_{k,z}$ from K nodes that $\boldsymbol{\theta} = [\boldsymbol{\theta}_1, \ldots, \boldsymbol{\theta}_K]^T$ in which

$$\boldsymbol{\theta}_k = [\theta_{k,x}, \theta_{k,z}]^T = [\theta_{k,x}^o, \theta_{k,z}^o]^T + [v_{k,x}, v_{k,z}]^T, \\ k \in [1, \ldots, K], \tag{5}$$

where $\theta_{k,x}^o$ and $\theta_{k,z}^o$ are the true values of $\theta_{k,x}$ and $\theta_{k,z}$ respectively. $v_{k,x} \sim \mathcal{N}\left(0, \sigma_{k,x}^2\right)$ and $v_{k,z} \sim \mathcal{N}\left(0, \sigma_{k,z}^2\right)$ are the independent Gaussian noise.

The advantage of using the projected angle as measurement is that the relationship between the measurement and the current frame can be simplified, which will be explained in the following contents.

III. MAXIMUM LIKELIHOOD ESTIMATOR FOR DoA-BASED RBL FRAMEWORK

To estimate the rotation matrix and the translation vector, which respectively present the attitude and the position of the rigid target, three maximum likelihood estimators are introduced in this section.

The proposed three MLEs calculate the rotation matrix and the translation vector from different perspectives. The first algorithm is to find the position of the rigid body first, and then use the unit quaternion to find the translation vector and the rotation matrix. The other two directly find the translation vector and the rotation matrix by considering them as unknowns.

A. TOPOLOGY MATCHING MAXIMUM LIKELIHOOD ESTIMATOR

The first MLE is divided into two phases: establishing the MLE to calculate the 3D coordinates of the nodes in the current frame and then points matching techniques to find $\mathbf{R}$ and $\mathbf{t}$.

We use the projected angle as a measurement is to simplify the relationship between $\boldsymbol{\theta}_k$ and $\mathbf{s}_k$ in the current frame

$$\mathbf{s}_k = [\tan\theta_{k,x}, 1, \tan\theta_{k,z}]^T * s_{y,k}. \tag{6}$$

In this way, we decrease the $3 \times K$ unknowns of the current frame into $1 \times K$ unknowns, i.e. $\boldsymbol{\phi}_1 = \mathbf{s}_y = [s_{y,1}, \ldots, s_{y,k}, \ldots, s_{y,K}]^T$. The exactly known topology of the wireless nodes is utilized, in addition to known measured angle information. We assume the $\frac{K(K-1)}{2}$ accurate node distance is subject to zero-mean white Gaussian noise with a quite small variance $\varepsilon_{i,j}^2$. Then, the maximum likelihood function of $\mathbf{d}$ can be shown as

$$p(\mathbf{d}; \boldsymbol{\phi}_1) = \frac{1}{\sqrt{\prod_{i=2}^{K} \prod_{j=1}^{i} 2\pi\varepsilon_{i,j}^2}}$$
$$\times \exp\left[-\frac{1}{2}(\mathbf{d_o} - \mathbf{d}(\boldsymbol{\phi}_1))^T \mathbf{W_d}^{-1}(\mathbf{d_o} - \mathbf{d}(\boldsymbol{\phi}_1))\right], \tag{7}$$

where $\mathbf{W_d} = \text{diag}(\varepsilon_{1,2}^2, \ldots \varepsilon_{i,j}^2, \ldots, \varepsilon_{K-1,K}^2)$ is the covariance square matrix of node-pair distance measurement noise and all $\varepsilon_{i,j}^2$ can be replaced by a small constant, say 10^{-5} meter, when we assume the confidence of the node pair distances is the same high. Then the ML estimator of the parameter $\mathbf{s}_y$ is the minimizer of the cost function

$$\mathcal{L}_1 = (\mathbf{d_o} - \mathbf{d}(\boldsymbol{\phi}_1))^T \mathbf{W_d}^{-1}(\mathbf{d_o} - \mathbf{d}(\boldsymbol{\phi}_1)). \tag{8}$$

From Gauss-Newton's method, we can find the solution of $\mathbf{s}_y$, and the coordinates of the wireless nodes in the current

frame will be obtained by substituting $\mathbf{s}_y$ into (6). At last, the translation vector and the rotation matrix can be obtained with all known information by the unit quaternion method or the SVD method.

As described above, the topology matching maximum likelihood estimator realizes the RBL by obtaining K sensors' $\mathbf{s}_y$ coordinates, while the matching information is the $K(K-1)/2$ distances. In this article, we consider $K = 4$ and there are 6 conditions and 4 unknowns thereby we also term this estimator as MLE64.

B. MEASUREMENT MATCHING MAXIMUM LIKELIHOOD ESTIMATOR

The second estimator is designed to find the rotation angle and the translation vector. Since we have the node pair distance information, the reference frame can be calculated by MDS algorithm (in the simulation work of this article, the reference frame is predetermined, instead of using MDS algorithm to fuse the node pair distance for getting the reference frame, which is a more general method).

The Rotation matrix can be defined with three Euler angles $\boldsymbol{\gamma} = [\varphi_p, \varphi_y, \varphi_r]^T$ where $\varphi_p, \varphi_y, \varphi_r$ are pitch, yaw, roll, respectively. We define the rotation matrix as a vector of 3×1 that

where $c*$ is $\cos*$ and $s*$ presents $\sin*$.

Thus, including the translation vector $\mathbf{t} = (x, y, z)^T$, there are 6 unknowns $\boldsymbol{\phi}_2 = [\boldsymbol{\gamma}^T, \mathbf{t}^T]^T$. as the distance is already fused for obtaining the reference frame, the only available condition is the DoA measurement. K nodes result in $2 \times K$ DoAs. According to (1) and (6), The relationship between the DoA measurement and the 6 unknowns can be expressed as $\boldsymbol{\theta} = \boldsymbol{\theta}(\boldsymbol{\phi}_2)$, which is specified as

$$\boldsymbol{\theta}_k = [\theta_{k,x}, \theta_{k,z}]^T = \arctan[s_{x,k}/s_{y,k}, s_{z,k}/s_{y,k}]^T$$
$$= \arctan\left[\frac{\mathbf{r}_1(\boldsymbol{\phi}_2)\mathbf{c}_k + x}{\mathbf{r}_2(\boldsymbol{\phi}_2)\mathbf{c}_k + y}, \frac{\mathbf{r}_3(\boldsymbol{\phi}_2)\mathbf{c}_k + z}{\mathbf{r}_2(\boldsymbol{\phi}_2)\mathbf{c}_k + y}\right]^T. \tag{10}$$

As the DoAs are independently measured and mixed with zero-mean white Gaussian noise (see (6)), the maximum likelihood function of $\boldsymbol{\theta}$ can be shown as

$$p(\mathbf{d}; \boldsymbol{\phi}_2) = \frac{1}{\sqrt{\prod_{k=1}^{K} 2\pi\sigma_{k,x}^2 \prod_{k=1}^{K} 2\pi\sigma_{k,z}^2}}$$
$$\times \exp\left[-\frac{1}{2}(\tilde{\boldsymbol{\theta}}_\mathbf{o} - \tilde{\boldsymbol{\theta}}(\boldsymbol{\phi}_2))^T \mathbf{W}_{\tilde{\boldsymbol{\theta}}}^{-1}(\tilde{\boldsymbol{\theta}}_\mathbf{o} - \tilde{\boldsymbol{\theta}}(\boldsymbol{\phi}_2))\right], \tag{11}$$

where $\tilde{\boldsymbol{\theta}}_\mathbf{o}$ and $\tilde{\boldsymbol{\theta}}$ are the vectors obtained by $\tilde{\boldsymbol{\theta}}_o = [\boldsymbol{\theta}_{o1}^T, \ldots, \boldsymbol{\theta}_{oK}^T]^T$ and $\boldsymbol{\theta} = [\boldsymbol{\theta}_{o1}^T, \ldots, \boldsymbol{\theta}_K^T]^T$ respectively; $\mathbf{W}_{\tilde{\boldsymbol{\theta}}} = \text{diag}(\sigma_{1,x}^2, \sigma_{1,z}^2, \ldots, \sigma_{K,x}^2, \sigma_{K,z}^2)$ is the noise covariance

$$\mathbf{R} = [\mathbf{r}_1, \mathbf{r}_2, \mathbf{r}_3]^T$$
$$= \begin{bmatrix} c\varphi_r c\varphi_p - s\varphi_r s\varphi_y s\varphi_p & -s\varphi_r c\varphi_y & c\varphi_r s\varphi_p + s\varphi_r s\varphi_y c\varphi_p \\ -s\varphi_r c\varphi_p - c\varphi_r s\varphi_y s\varphi_p & -c\varphi_r c\varphi_y & -s\varphi_r s\varphi_p + c\varphi_r s\varphi_y c\varphi_p \\ -c\varphi_y s\varphi_p & s\varphi_y & c\varphi_y c\varphi_p \end{bmatrix}, \tag{9}$$

matrix of DoA measurement noise. The ML estimator of parameter $\gamma, \mathbf{t}$ is the minimizer of the cost function

$$\mathcal{L}_2 = (\tilde{\boldsymbol{\theta}}_{\mathbf{o}} - \tilde{\theta}(\boldsymbol{\phi}_2))^T \mathbf{W}_{\tilde{\boldsymbol{\theta}}}^{-1}(\tilde{\boldsymbol{\theta}}_{\mathbf{o}} - \tilde{\theta}(\boldsymbol{\phi}_2)). \quad (12)$$

After the optimal $\boldsymbol{\phi}_2$ is obtained, we substitute γ into Equation (9), as shown at the bottom of the previous page, and get $\mathbf{R}$, which finishes the $\mathbf{t}$ and $\mathbf{R}$ estimation.

The estimator of (12) exploits the 2-D DoA measurements as conditions, the arguments to be estimated are the rotation angles γ and $\mathbf{t}$. When $K = 4$, 8 are used to seek for 6 arguments. In this perspective, we also term the estimator (12) as MLE86 for sake of simplicity.

C. CONSTRAINT-MEASUREMENT MATCHING MAXIMUM LIKELIHOOD ESTIMATOR

Similar to the measurement matching maximum likelihood estimator discussed above, we focus on the affine transformation of (1), which means the reference frame fused with topology information has already predetermined. To mitigate the non-linearity, we consider directly the matrix elements instead of the rotation angle. If we estimate the rotation matrix and translation vector directly, there will be 12 unknowns, including a 3×3 rotation matrix and a 1×3 translation vector. The argument vector is given as $\boldsymbol{\phi}_3 = \left[\mathbf{r}_1^T, \mathbf{r}_2^T, \mathbf{r}_3^T, \mathbf{t}^T\right] \in \mathbb{R}^{12 \times 1}$.

The conditions used for estimating $\boldsymbol{\phi}_3$ includes the DoA measurements and the equality constraint. We rewrite Equation (10) to express the mathematical relationship between $\boldsymbol{\phi}_3$ and the DoA measurement as

$$\boldsymbol{\theta}_k = \left[\theta_{k,x}, \theta_{k,z}\right]^T$$
$$= \arctan\left[s_{x,k}(\boldsymbol{\phi}_3)/s_{y,k}(\boldsymbol{\phi}_3), s_{z,k}(\boldsymbol{\phi}_3)/s_{y,k}(\boldsymbol{\phi}_3)\right]^T. \quad (13)$$

The relationship between $s_{x,k}$, $s_{y,k}$, $s_{z,k}$, and $\boldsymbol{\phi}_3$ is revealed by Equation (1) and (9). From the constraint of $SO(3)$ in (2), we can specify the constrain into equations:

$$\left[\mathbf{r}_1^T\mathbf{r}_1 - 1, \mathbf{r}_2^T\mathbf{r}_2 - 1, \mathbf{r}_3^T\mathbf{r}_3 - 1, \mathbf{r}_1^T\mathbf{r}_2, \mathbf{r}_1^T\mathbf{r}_3, \mathbf{r}_2^T\mathbf{r}_3\right]^T$$
$$= \boldsymbol{\lambda} = [\lambda_1, \ldots, \lambda_6]^T. \quad (14)$$

Actually, $\boldsymbol{\lambda}$ equals $\mathbf{0}_{6 \times 1}$, according (2). However, when we are finding the optimal $\boldsymbol{\phi}_3$, it is assumed $\boldsymbol{\lambda}$ is mixed with zero-meaning additional Gaussian noise. This assumption is reasonable when the variance is set as much small constant. In this way, the ground truth of the employed conditions is denoted by $\boldsymbol{\Gamma}_{\mathbf{o}} = [\tilde{\boldsymbol{\theta}}_o^T, \mathbf{0}_{1 \times 6}]^T \in \mathbb{R}^{(2K+6) \times 1}$, while the likelihood function of $\boldsymbol{\Gamma}(\boldsymbol{\phi}_3) = [\tilde{\theta}(\boldsymbol{\phi}_3)^T, \boldsymbol{\lambda}(\boldsymbol{\phi}_3)^T]^T$ can be shown as

$$p\left(\mathbf{d}; \boldsymbol{\phi}_2\right) = \frac{1}{\sqrt{\prod_{n=1}^{6} 2\pi \varepsilon^2 \prod_{k=1}^{K} 2\pi \sigma_{k,x}^2 \prod_{k=1}^{K} 2\pi \sigma_{k,z}^2}}$$
$$\times \exp\left[-\frac{1}{2}(\boldsymbol{\Gamma}_{\mathbf{o}} - \boldsymbol{\Gamma}(\boldsymbol{\phi}_3))^T \mathbf{W}_{\boldsymbol{\Gamma}}^{-1}(\boldsymbol{\Gamma}_{\mathbf{o}} - \boldsymbol{\Gamma}(\boldsymbol{\phi}_3))\right], \quad (15)$$

where $\mathbf{W}_{\boldsymbol{\Gamma}}$ is the noise covariance matrix. Considering the elements in $\boldsymbol{\Gamma}$ are independent information, $\mathbf{W}_{\boldsymbol{\Gamma}}$ can
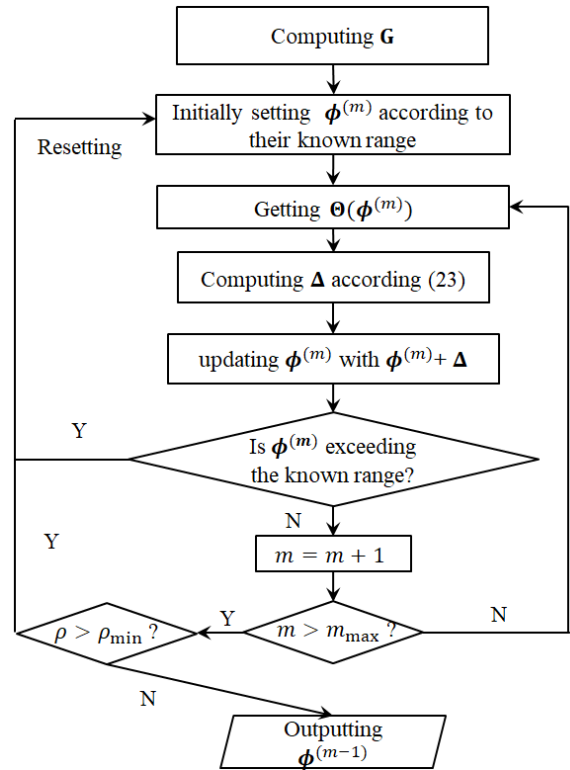

FIGURE 2. The modified Gauss-Newton algorithm with an additional convergence quality checking.

be given as

$$\mathbf{W}_{\boldsymbol{\Gamma}} = \text{diag}(\sigma_{1,x}^2, \sigma_{1,z}^2, \ldots, \sigma_{K,x}^2, \sigma_{K,z}^2, \varepsilon^2 \otimes \mathbf{1}_{6 \times 1}). \quad (16)$$

ε^2 equals 0 since λ equals $\mathbf{0}_{6 \times 1}$ for sure. But we should give ε^2 a non-zero value for guaranteeing that $\mathbf{W}_{\boldsymbol{\Gamma}}$ be a full-rank matrix. But ε^2 should be set much smaller than $\sigma_{k,x}^2$ or $\sigma_{k,z}^2$, which is practically measured with noise. The ML estimator of parameter $\gamma, \mathbf{t}$ is the minimizer of the cost function.

$$\mathbf{L}_3 = (\boldsymbol{\Gamma}_{\mathbf{o}} - \boldsymbol{\Gamma}(\boldsymbol{\phi}_3))^T \mathbf{W}_{\boldsymbol{\Gamma}}^{-1}(\boldsymbol{\Gamma}_{\mathbf{o}} - \boldsymbol{\Gamma}(\boldsymbol{\phi}_3)). \quad (17)$$

After obtaining the optimal $\boldsymbol{\phi}_3$, we finish the $\mathbf{t}$ and $\mathbf{R}$ estimation.

In (12), when $K = 4$, there are 14 conditions, including 8 DoAs and 6 constraint equalities, while the parameters to be estimated is 12, Therefore, we term this estimator as MLE1412.

Here, it is important to note that above all three MLEs need more than three wireless nodes in the SSWSN for completing the RBL task; this is a clear conclusion by analyzing the numbers of employed conditions and estimated parameters.

IV. MODIFIED GAUSSIAN-NEWTON ALGORITHM FOR MLEs

For finding the optimal solution that minimizes the cost function (8), (12) and (17), many optimization methodologies can be adopted. Here we apply the Gaussian-Newton algorithm to complete this task. The basic idea of Gauss-Newton iterative method is to use Taylor series expansion to approximate

the nonlinear regression model, and then through multiple iterations, modify the regression coefficient for many times, so that the regression coefficient continuously approximates the best regression coefficient of the nonlinear regression model, and finally make the sum of squares of the residual error of the original model.

The above three MLEs can be generally expressed as

$$\mathbf{L} = (\mathbf{\Theta_o} - \mathbf{\Theta}(\boldsymbol{\phi}))^T \mathbf{W}^{-1} (\mathbf{\Theta_o} - \mathbf{\Theta}(\boldsymbol{\phi})), \quad (18)$$

where $\mathbf{\Theta_o}$ represents the information vector, i.e., $\mathbf{d_o}$, $\tilde{\boldsymbol{\theta}}_\mathbf{o}$ and $\mathbf{\Gamma_o}$; $\boldsymbol{\phi}$ represents the vectorized parameters to be estimated, i.e., $\boldsymbol{\phi}_1$, $\boldsymbol{\phi}_2$ and $\boldsymbol{\phi}_3$; $\mathbf{W}$ is the symbol of $\mathbf{W_d}$, $\mathbf{W}_{\tilde{\theta}}$ and $\mathbf{W_\Gamma}$. Because all the conditions are considered as following the Gaussian distribution, the MLEs of the above three RBL methods can be regarded as weighted least square estimator. To translate (18) into common least square estimator, we use $\mathbf{\Theta_o^*} = \mathbf{V}\mathbf{\Theta_o}$ and $\mathbf{\Theta}^*(\boldsymbol{\phi}) = \mathbf{V}\mathbf{\Theta}(\boldsymbol{\phi})$, in which $\mathbf{V} = \sqrt{\mathbf{W}}^{-1}$, thereby (18) can be rewritten as

$$\mathbf{L} = (\mathbf{\Theta_o^*} - \mathbf{\Theta}^*(\boldsymbol{\phi}))^T (\mathbf{\Theta_o^*} - \mathbf{\Theta}^*(\boldsymbol{\phi})), \quad (19)$$

which is a nonlinear least square problem.

To linearize the least square problem, at the initial value $\boldsymbol{\phi}^{(0)}$ and ignoring the items whose order are higher than two, and we can obtain

$$\mathbf{\Theta_o^*} - \mathbf{\Theta}^*(\boldsymbol{\phi}) \approx \mathbf{\Theta_o^*} - \mathbf{\Theta}^*\left(\boldsymbol{\phi}^{(0)}\right) + \mathbf{G}^* \cdot \left(\boldsymbol{\phi} - \boldsymbol{\phi}^{(0)}\right), \quad (20)$$

where $\mathbf{G}^* = \mathbf{V}\mathbf{G}$. $\mathbf{G}$ is the Jacobian matrix $\mathbf{G} = \frac{\partial \mathbf{\Theta}(\boldsymbol{\phi})}{\partial \boldsymbol{\phi}}$. For the three MLEs, $\mathbf{G}$ can respectively be calculated by

$$\mathbf{G_1} = \frac{\partial \mathbf{d}^T}{\partial \mathbf{s}_y} = \begin{bmatrix} \frac{\partial d_{1,2}}{\partial y_1} & \cdots & \frac{\partial d_{1,2}}{\partial y_K} \\ \vdots & \vdots & \vdots \\ \frac{\partial d_{i,j}}{\partial y_1} & \cdots & \frac{\partial d_{i,j}}{\partial y_K} \\ \vdots & \vdots & \vdots \\ \frac{\partial d_{K-1,K}}{\partial y_1} & \cdots & \frac{\partial d_{K-1,K}}{\partial y_K} \end{bmatrix}$$
$$\in R^{\frac{(K-1)K}{2} \times K}, \quad (21)$$

$$\mathbf{G_2} = \left[\frac{\partial \boldsymbol{\theta}(\boldsymbol{\phi}_2)}{\partial \boldsymbol{\gamma}}, \frac{\partial \boldsymbol{\theta}(\boldsymbol{\phi}_2)}{\partial \mathbf{t}} \right]$$
$$= \begin{bmatrix} \frac{\partial \theta_{1,x}}{\partial x} & \frac{\partial \theta_{1,x}}{\partial y} & \frac{\partial \theta_{1,x}}{\partial z} & \frac{\partial \theta_{1,x}}{\partial \varphi_p} & \frac{\partial \theta_{1,x}}{\partial \varphi_y} & \frac{\partial \theta_{1,x}}{\partial \varphi_r} \\ \frac{\partial \theta_{1,z}}{\partial x} & \frac{\partial \theta_{1,z}}{\partial y} & \frac{\partial \theta_{1,z}}{\partial z} & \frac{\partial \theta_{1,z}}{\partial \varphi_p} & \frac{\partial \theta_{1,z}}{\partial \varphi_y} & \frac{\partial \theta_{1,z}}{\partial \varphi_r} \\ & & \vdots & \vdots & & \\ \frac{\partial \theta_{K,x}}{\partial x} & \frac{\partial \theta_{K,x}}{\partial y} & \frac{\partial \theta_{K,x}}{\partial z} & \frac{\partial \theta_{K,x}}{\partial \varphi_p} & \frac{\partial \theta_{K,x}}{\partial \varphi_y} & \frac{\partial \theta_{K,x}}{\partial \varphi_r} \\ \frac{\partial \theta_{K,z}}{\partial x} & \frac{\partial \theta_{K,z}}{\partial y} & \frac{\partial \theta_{K,z}}{\partial z} & \frac{\partial \theta_{K,z}}{\partial \varphi_p} & \frac{\partial \theta_{K,z}}{\partial \varphi_y} & \frac{\partial \theta_{K,z}}{\partial \varphi_r} \end{bmatrix}$$
$$\in R^{2K \times 6}, \quad (22)$$

and

$$\mathbf{G_3} = \left[\frac{\partial \mathbf{\Gamma}(\boldsymbol{\phi}_3)}{\partial \boldsymbol{\phi}_3} \right]$$
$$= \begin{bmatrix} \frac{\partial \theta_{1,x}}{\partial x} & \frac{\partial \theta_{1,x}}{\partial y} & \frac{\partial \theta_{1,x}}{\partial z} & \frac{\partial \theta_{1,x}}{\partial r_{1,1}} & \cdots & \frac{\partial \theta_{1,x}}{\partial r_{3,3}} \\ \frac{\partial \theta_{1,z}}{\partial x} & \frac{\partial \theta_{1,z}}{\partial y} & \frac{\partial \theta_{1,z}}{\partial z} & \frac{\partial \theta_{1,z}}{\partial r_{1,1}} & \cdots & \frac{\partial \theta_{1,z}}{\partial r_{3,3}} \\ & \vdots & & & \vdots & \\ \frac{\partial \theta_{K,x}}{\partial x} & \frac{\partial \theta_{K,x}}{\partial y} & \frac{\partial \theta_{K,x}}{\partial z} & \frac{\partial \theta_{K,x}}{\partial r_{1,1}} & \cdots & \frac{\partial \theta_{K,x}}{\partial r_{3,3}} \\ \frac{\partial \theta_{K,z}}{\partial x} & \frac{\partial \theta_{K,z}}{\partial y} & \frac{\partial \theta_{K,z}}{\partial z} & \frac{\partial \theta_{K,z}}{\partial r_{1,1}} & \cdots & \frac{\partial \theta_{K,z}}{\partial r_{3,3}} \\ \frac{\partial \lambda_1}{\partial x} & \frac{\partial \lambda_1}{\partial y} & \frac{\partial \lambda_1}{\partial z} & \frac{\partial \lambda_1}{\partial r_{1,1}} & \cdots & \frac{\partial \lambda_1}{\partial r_{3,3}} \\ & \vdots & & & \vdots & \\ \frac{\partial \lambda_6}{\partial x} & \frac{\partial \lambda_6}{\partial y} & \frac{\partial \lambda_6}{\partial z} & \frac{\partial \lambda_6}{\partial r_{1,1}} & \cdots & \frac{\partial \lambda_6}{\partial r_{3,3}} \end{bmatrix}$$
$$\in R^{\left(2K + \frac{(K-1)K}{2}\right) \times 12}. \quad (23)$$

At m-th iteration, the gap between the current information vector $\boldsymbol{\phi}^{(m)}$ and the optimal solution $\boldsymbol{\phi}$ can be obtained from Equation (20) that

$$\Delta = \boldsymbol{\phi} - \boldsymbol{\phi}^{(m)} = \left(\mathbf{G}^{*T}\mathbf{G}^*\right)^{-1} \mathbf{G}^{*T} \left(\mathbf{\Theta_o} - \mathbf{\Theta}\left(\boldsymbol{\phi}^{(m)}\right)\right)$$
$$= \left(\mathbf{G}^T \mathbf{W}^{-1} \mathbf{G}\right)^{-1} \mathbf{W}^{-\frac{1}{2}} \mathbf{G}^T (\mathbf{\Theta_o} - \mathbf{\Theta}\left(\boldsymbol{\phi}^{(m)}\right)). \quad (24)$$

Then at next iteration, we can update the iterative value by replacing $\boldsymbol{\phi}^{(m+1)} = \boldsymbol{\phi}^{(m)} + \Delta$. The above iteration will be stopped until the optimization convergences that $\Delta^T \Delta$ is decreased below a small threshold or the maximum number of iterations has been reached.

Empirically, the traditional Newton's method is easy to get into the local optimum when the initial value $\boldsymbol{\phi}^{(0)}$ is not nearby the ground truth because the models of interest are non-convex. Thus, we modify the classic Newton's method by adding the criterion of the convergence quality. After stopping the iteration, we will compute the similarity ρ between the information vector yielded from the final $\boldsymbol{\phi}^{(max)}$ and the information vector measured by $\rho = \left\| \mathbf{\Theta_o} - \mathbf{\Theta}\left(\boldsymbol{\phi}^{(m)}\right) \right\|$. If ρ is larger than the predetermined threshold, which means that the convergence is stuck in the local optimal solution, we will discard the convergence result and reset $\boldsymbol{\phi}$ by randomly setting $\boldsymbol{\phi}^{(0)}$ according to the apriori knowledge, and begin the Newton iteration again.

Essentially, the space-related parameters to be estimated include $\mathbf{s}_y$ for the MLE64 and $\mathbf{t}$ for the MLE86 and MLE1412. As the apriori knowledge of the space-related parameters, their ranges can be roughly determined according to the room size of the monitoring area or can be measured through the RSS indicator. Besides, the range of the Euler angles $\boldsymbol{\gamma}$ for MLE86 is obviously from 0 to 2π, and the elements of $\mathbf{R}$ for MLE1412 belong to $0 \sim 1$.
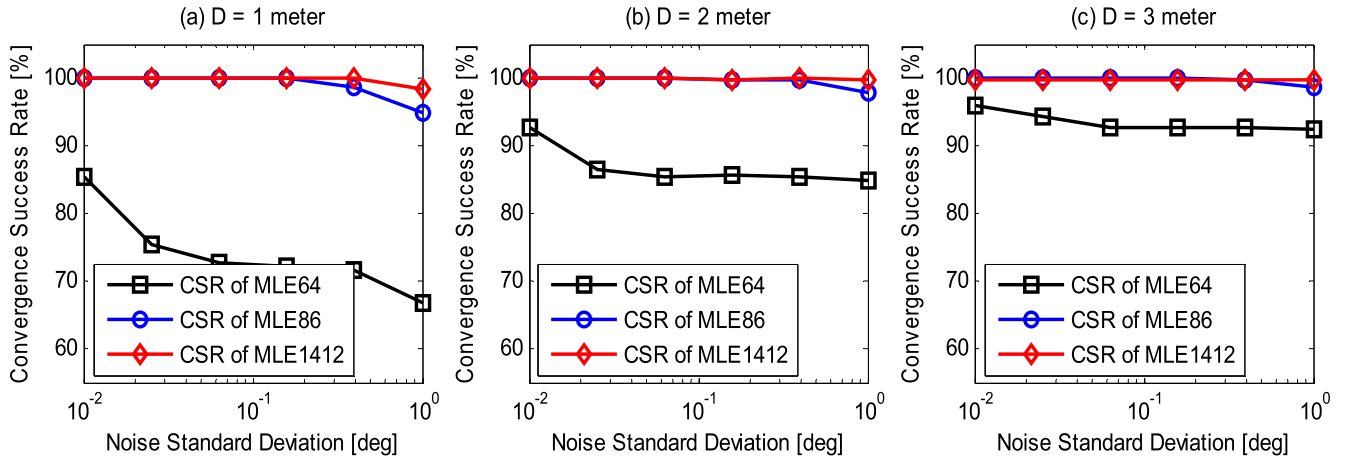
FIGURE 3. The convergence success rate of three MLEs under different noise standard deviation and rigid target sizes.

TABLE 1. Simulation parameters.

PARAMETERS	DESCRIPTION
σ^2	Noise variance of DoA measurement
CSR	convergence success rates
D	Size of the rigid target of interest
RMSE	Accuracy of $\mathbf{t}$ and $\mathbf{R}$ estimation

TABLE 2. The computational cost when $D = 2$ meter.

	MLE64	MLE86	MLE1412
$\sigma^2 = 10^0$ deg	71.5 ms	4.8 ms	2.3 ms
$\sigma^2 = 10^{-1}$ deg	85.6 ms	7.1 ms	2.2 ms
$\sigma^2 = 10^{-2}$ deg	88.5 ms	12.7 ms	2.3 ms

If ρ cannot reach the threshold, the whole parameter estimating process will be quitted after resetting the initial value 500 times.

V. PERFORMANCE EVALUATION

We conduct the simulation experiment using MATLAB on a personal computer with a 2.0 GHz Quad-Core Processor. We perform the simulation experiment under various situations (different body sizes D and different DoA measurement noise σ^2) to evaluate the three estimators, in terms of the convergence success rate (CSR) and the computational cost, as well as the Root Mean Square Error (RMSE).

For conveniently presenting the simulation performance evaluation, we provide the simulation parameters in Table 1:

We give the initial frame as follows:

$$\mathbf{C} = \begin{bmatrix} 0 & 1 & 0 & 0 \\ 0 & 0 & 1 & 0 \\ 0 & 0 & 0 & 1 \end{bmatrix} * D. \quad (25)$$

The apriori state information of the rigid target that, concerning to the initial frame, the current frame located in the 3-D space of $x \in [0, 8] \cap y \in [0, 8] \cap z \in [0, 6]$ meter and the single BS is located at the origin. Meanwhile, the three rotation angles are set randomly, belonging to $[0, 2\pi]$ to the reference frame.

Firstly, the robustness of three estimators is compared when $D = 1, 2, 3$ meter under 6 different noise levels. We launch 1000 independently Monte Carlo runs for each case, and in each run, the ground truth of $\mathbf{t}$ and $\mathbf{R}$ are selected randomly, and the initial solution of Newton's method is also selected randomly. Of cause, the ground truth and initial solution selections are both according to the known prior

information, then the estimated result is matched with the ground truth for judging the convergence success.

The convergence success rates (CSRs) of the three estimators are presented in Figure 3. As we expected, higher CSR will be achieved at a lower DoA noise level and bigger body size. The robustness of MLE1412 outperforms the other two MLEs. The CSR of MLE1412 always keeps approximating 100% even at the harshest case (the highest noise level $\sigma^2 = 1$ deg when $D = 1$ meter). This is a remarkable performance since it is known to all that Newton's method is quite fragile to the initial value. The MLE86 also obtains a rather good performance and the CSR is higher than 95% at a high noise level while the MLE64 offers fine performance only at low DoA noise level. Intuitively, the more conditions that were used (14 conditions for MLE1412, including 6 constraints and 8 DoA measurements; 8 conditions for MLE86, including 8 DoA measurements; 6 conditions for MLE64, including 6 node pair distances), the more robust the MLE is to measurement noises, from the point of Gaussian-Newton method.

Table 2 presents the computational cost of the RBL methods. In common sense, the higher dimensional of the parameters to be estimated, the slower the convergence process will be. However, it can be figured out that MLE1412 is the most efficient estimator. This is due to that its higher CSR reduces the number of the initial value reset in Newton's algorithm. On the contrary, MLE64 needs the largest computational resource. We can also notice that MLE86 is efficient at low-level measurement noise while its efficiency will be degraded when the noise increases. It is due to the lower resetting frequency of modified Newton algorithm (presented in Figure 2) applied to the MLE1412, which proves the efficiency of the MLE1412 from another aspects.
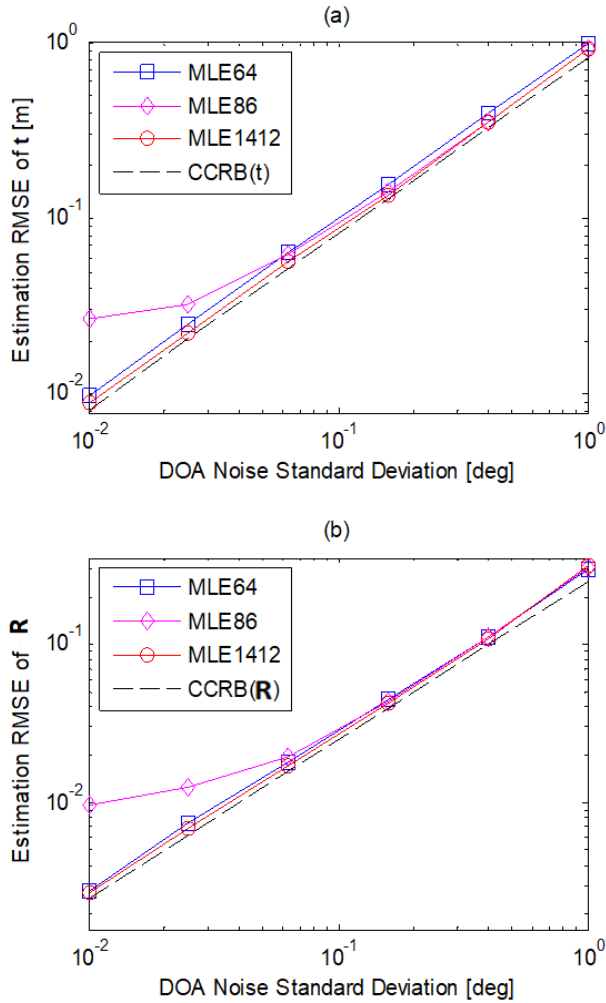
FIGURE 4. The RBL estimation comparison when $D = 1$ meter.

FIGURE 5. The RBL estimation comparison when $D = 3$ meter.

Secondly, we compare the RMSEs of all three MLEs to evaluate their RBL accuracy under different noise levels and body sizes. As ground truth, we preset the translate vector as $\mathbf{t} = [6, 5, 2]$ meter and assume the rotation angle to be $\boldsymbol{\gamma} = [-70 \, 55 \, 30]$ degree which resulting in

$$\mathbf{R} = \begin{bmatrix} 0.4967 & -0.2868 & 0.8192 \\ -0.4956 & 0.6811 & 0.5390 \\ -0.7125 & -0.6737 & 0.1962 \end{bmatrix}.$$

Under the above parameters, we provided corresponding CCRB as a benchmark and the detail of CCRB derivation can be found in [21].

Figures 4 and 5 illustrate the accuracy of all the estimators when $D = 1$ and $D = 3$. MLE1412 is the technique most approximating the CCRB, this means the assumption that the equality constraint of Equation (11) follows Gaussian distribution has not introduced much RBL estimation deviation. We select the result of successful convergence for MLE64 for comparison, but there is still an obvious gap between the MLE64 and the CCRB, especially for the small rigid-body size. This situation keeps consistent with the above analysis that more conditions used results in better performance.
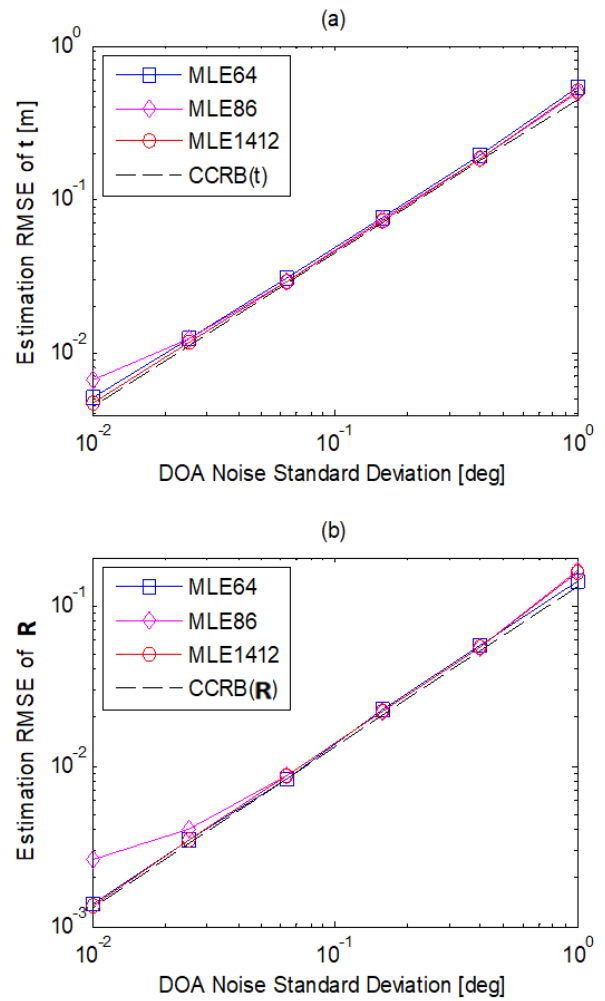
MLE86 can reach CCRB at higher level DoA noise but the performance gap is growing larger between the MLE86 and CCRB, which could be resulted by the high non-linearity during the translation between the rotation angle and the rotation matrix.

VI. CONCLUSION AND FUTURE WORK

In this paper, we proposed three maximum likelihood estimators for the DoA-based RBL framework via a single BS, which include matching topology information to estimate the nodes' coordinates in the current frame, using DoA measurements to find the optimal translation vector and the rotation angles, adopting DoA measurements and the constraint equalities to calculate the translation vector and the rotation matrix. Without loss of universality, we termed them MLE64, MLE86 and MLE1412, respectively, when the number of nodes is 4.

We optimized the three MLEs using the modified Newton-Gaussian algorithm, in which the initial value is reset regularly according to the apriori information for mitigating the convergence failure rate. Finally, the three MLEs are evaluated under different situations on convergence success rate, computational cost and accuracy. The result shows that

the RMSE of MLE1412 can approximate the CCRB while maintaining 100 percent convergence success rate under 1000 different situations. This performance is competent for most application situations, such as VR systems, space docking systems, etc. Besides, the computational cost is also acceptable for RBL schemes adopting single base station.

From this work, we assume the topology information is preciously known, which may not be satisfied when the rigid target is from the third party. Thus, in the future, we will study the effect of the noise topology information on the RBL performance, when we just roughly know the topology. It will be an interesting research topic that we only use the DoA measurement and rough topology information for calibrating the noisy topology information while accomplish the RBL task.

REFERENCES

[1] R. Featherstone, *Robot Dynamics Algorithms*. Cham, Switzerland: Springer, 2014.

[2] P. J. From, *Rigid Body Dynamics*. London, U.K.: Springer, 2014, pp. 191–227.

[3] X. Huang, W. Guo, G. Liu, and G. Chen, "FH-OAOS: A fast four-step heuristic for obstacle-avoiding octilinear steiner tree construction," *ACM Trans. Des. Autom. Electron. Syst.*, vol. 21, no. 3, pp. 1–31, Jul. 2016.

[4] X. Chen, A. Li, X. Zeng, W. Guo, and G. Huang, "Runtime model based approach to IoT application development," *Frontiers Comput. Sci.*, vol. 9, no. 4, pp. 540–553, Aug. 2015.

[5] F. L. Markley and J. L. Crassidi, *Fundamentals of Spacecraft Orientation Determination and Control*. New York, NY, USA: Springer-Verlag, 2014.

[6] J. Sauer, "A constraint-based approach to rigid body dynamics for virtual reality applications," in *Proc. Virtual Reality Softw. Technol.*, 1998, pp. 153–162.

[7] B. Lin, W. Guo, and N. Xiong, "A pretreatment workflow scheduling approach for big data applications in multicloud environments," *IEEE Trans. Netw. Service Manag.*, vol. 13, no. 3, pp. 581–594, Apr. 2016.

[8] C. Forster, L. Carlone, F. Dellaert, and D. Scaramuzza, "IMU preintegration on manifold for efficient visual-inertial maximum-a-posteriori estimation," in *Proc. Robot., Sci. Syst.*, Jul. 2015, pp. 1–5.

[9] Y. Niu, W. Lin, X. Ke, and L. Ke, "Fitting-based optimisation for image visual salient object detection," *IET Comput. Vis.*, vol. 11, no. 2, pp. 161–172, Mar. 2017.

[10] J. Simanek, M. Reinstein, and V. Kubelka, "Evaluation of the EKF-based estimation architectures for data fusion in mobile robots," *IEEE/ASME Trans. Mechatronics*, vol. 20, no. 2, pp. 985–990, Apr. 2015.

[11] M.-D. Hua, "Attitude estimation for accelerated vehicles using GPS/INS measurements," *Control Eng. Pract.*, vol. 18, no. 7, pp. 723–732, Jul. 2010.

[12] J.-C. Juang and G.-S. Huang, "Development of GPS-based attitude determination algorithms," *IEEE Trans. Aerosp. Electron. Syst.*, vol. 33, no. 3, pp. 968–976, Jul. 1997.

[13] Y. I. Abdel-Aziz and H. M. Karara, "Direct linear transformation from comparator coordinates into object space coordinates in close-range photogrammetry," *Photogrammetric Eng. Remote Sens.*, vol. 81, no. 2, pp. 103–107, Feb. 2015.

[14] X. Li, Z. Zhu, and W. Zhu, "Discrete relaxation method for triple patterning lithography layout decomposition," *IEEE Trans. Comput.*, vol. 66, no. 2, pp. 285–298, Feb. 2017.

[15] X. Li and W. Zhu, "Two-stage layout decomposition for hybrid E-beam and triple patterning lithography," *ACM Trans. Des. Autom. Electron. Syst.*, vol. 23, no. 1, pp. 1–23, Oct. 2017.

[16] D. W. Eggert, A. Lorusso, and R. B. Fisher, "Estimating 3-D rigid body transformations: A comparison of four major algorithms," *Mach. Vis. Appl.*, vol. 9, pp. 5–6, pp. 272–290, 1997.

[17] S. P. Chepuri, G. Leus, and A.-J. van der Veen, "Position and orientation estimation of a rigid body: Rigid body localization," in *Proc. IEEE Int. Conf. Acoust., Speech Signal Process.*, May 2013, pp. 5185–5189.

[18] S. P. Chepuri, G. Leus, and A.-J. van der Veen, "Rigid body localization using sensor networks," *IEEE Trans. Signal Process.*, vol. 62, no. 18, pp. 4911–4924, Sep. 2014.

[19] S. Chen and K. C. Ho, "Accurate localization of a rigid body using multiple sensors and landmarks," *IEEE Trans. Signal Process.*, vol. 63, no. 24, pp. 6459–6472, Dec. 2015.

[20] J. Jiang, G. Wang, and K. C. Ho, "Sensor network-based rigid body localization via semi-definite relaxation using arrival time and Doppler measurements," *IEEE Trans. Wireless Commun.*, vol. 18, no. 2, pp. 1011–1025, Feb. 2019.

[21] B. Zhou, L. Ai, X. Dong, and L. Yang, "DoA-based rigid body localization adopting single base station," *IEEE Commun. Lett.*, vol. 23, no. 3, pp. 494–497, Mar. 2019.

[22] G. Wang and K. C. Ho, "Accurate semidefinite relaxation method for 3-D rigid body localization using AOA," in *Proc. IEEE Int. Conf. Acoust., Speech Signal Process. (ICASSP)*, May 2020, pp. 4955–4959.

[23] B. Lin, W. Guo, and X. Lin, "Online optimization scheduling for scientific workflows with deadline constraint on hybrid clouds," *Concurrency Comput., Pract. Exper.*, vol. 28, no. 11, pp. 3079–3095, Aug. 2016.

[24] Y. Xia and J. Wang, "A bi-projection neural network for solving constrained quadratic optimization problems," *IEEE Trans. Neural Netw. Learn. Syst.*, vol. 27, no. 2, pp. 214–224, Feb. 2016.

[25] Z. He, "Evolutionary K-means with pair-wise constraints," *Soft Comput.*, vol. 20, no. 1, pp. 287–301, 2016.

[26] Y. Xia, H. Leung, and M. S. Kamel, "A discrete-time learning algorithm for image restoration using a novel L2-norm noise constrained estimation," *Neurocomputing*, vol. 198, pp. 155–170, Jul. 2016.

[27] W. Guo, J. Li, G. Chen, Y. Niu, and C. Chen, "A PSO-optimized real-time fault-tolerant task allocation algorithm in wireless sensor networks," *IEEE Trans. Parallel Distrib. Syst.*, vol. 26, no. 12, pp. 3236–3249, Dec. 2015.

[28] W. Guo, G. Liu, G. Chen, and S. Peng, "A hybrid multi-objective PSO algorithm with local search strategy for VLSI partitioning," *Frontiers Comput. Sci.*, vol. 8, no. 2, pp. 203–216, Apr. 2014.

[29] G. Liu, W. Guo, Y. Niu, G. Chen, and X. Huang, "A PSO-based timing-driven octilinear steiner tree algorithm for VLSI routing considering bend reduction," *Soft Comput.*, vol. 19, no. 5, pp. 1153–1169, May 2015.

[30] W. Guo, G. Liu, G. Chen, and S. Peng, "A hybrid multi-objective PSO algorithm with local search strategy for VLSI partitioning," *Frontiers Comput. Sci.*, vol. 8, no. 2, pp. 203–216, Apr. 2014.

[31] X. Huang, G. Liu, W. Guo, Y. Niu, and G. Chen, "Obstacle-avoiding algorithm in X-Architecture based on discrete particle swarm optimization for VLSI design," *ACM Trans. Des. Autom. Electron. Syst.*, vol. 20, no. 2, pp. 1–28, Mar. 2015.

[32] G. Liu, W. Guo, R. Li, Y. Niu, and G. Chen, "XGRouter: High-quality global router in X-architecture with particle swarm optimization," *Frontiers Comput. Sci.*, vol. 9, no. 4, pp. 576–594, Aug. 2015.

[33] K. Aghababaiyan, R. G. Zefreh, and V. Shah-Mansouri, "3D-OMP and 3D-FOMP algorithms for DOA estimation," *Phys. Commun.*, vol. 31, pp. 87–95, Dec. 2018.
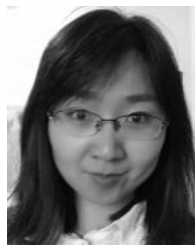
LINGYU AI received the B.S. degree from the Qingdao University of Science and Technology, China, in 2012, and the Ph.D. degree from Kwangwoon University, Seoul, South Korea, in 2018. She is currently working as a Lecturer with the School of Internet of Things Engineering, Jiangnan University, Wuxi, China. Her research interests include 3D positioning techniques, image signal processing, and integral imaging systems.

CHANGQIANG JING received the B.S. degree from the Qingdao University of Science and Technology, China, in 2008, and the Ph.D. degree from Kwangwoon University, Seoul, South Korea, in 2015. He joined the School of Informatics, Linyi University, China, as a Faculty Member, in 2015. His research interests include ultra-wideband systems, embedded systems, and high accuracy positioning systems.

YEHCHENG CHEN is currently pursuing the Ph.D. degree with the Department of Computer Science, University of California at Davis, Davis, CA, USA. His research interests include radio-frequency identification (RFID), data mining, social networks, information systems, wireless network artificial intelligence, the IoT, and security.

SHENGLAN WU is currently pursuing the master's degree with the School of Internet of Things Engineering, Jiangnan University. Her research interests include passive positioning with satellite and rigid body localization.

TAO ZHANG (Member, IEEE) received the bachelor's degree from Henan Polytechnic University, Jiaozuo, China, in 2008, and the Ph.D. degree from the Institute of Image Processing and Pattern Recognition, Shanghai Jiao Tong University, Shanghai, China, in 2016. He is currently an Associate Professor with the Jiangsu Provincial Engineering Laboratory for Pattern Recognition and Computational Intelligence, Jiangnan University, Wuxi, China. He has led many research projects, such as the National Science Foundation and the National Joint Fund. He has authored over thirty quality journal articles and conference papers. His current research interests include medical image processing, medical data analysis, visual surveillance, scene understanding, behavior analysis, object detection, and pattern analysis.

• • •